Journal of ELECTRONIC MATERIALS, Vol. 43, No. 9, 2014
DOI: 10.1007/s11664-014-3183-5

Structural and Optical Characterizations of Electrochemically Grown Connected and Free-Standing TiO_2 Nanotube Array

A. HAZRA,[1] K. DUTTA,[1] B. BHOWMIK,[1] V. MANJULADEVI,[2] R.K. GUPTA,[2] P.P. CHATTOPADHYAY,[3] and P. BHATTACHARYYA[1,4]

1.—Nano-Thin Films and Solid State Gas Sensor Devices Laboratory, Department of Electronics and Telecommunication Engineering, Indian Institute of Engineering Science and Technology, Shibpur, Howrah 711103, India. 2.—Department of Physics, Birla Institute of Technology and Science, Pilani 333031, Rajasthan, India. 3.—Department of Metallurgy and Materials Engineering, Indian Institute of Engineering Science and Technology, Shibpur, Howrah 711103, India. 4.—e-mail: pb_etc_besu@yahoo.com

A TiO_2 nanotube array was grown electrochemically by using single and mixed electrolyte/s with 20 V constant potential at room temperature. Anodization was carried out for 120 min using five different electrolytes, e.g., H_3PO_4, NH_4F, HF, NH_4F with H_3PO_4 and HF with H_3PO_4. Structural characterizations of the grown titania nanotubes were conducted by using x-ray diffraction and field emission scanning electron microscopy. Optical properties of the grown nanotubes were investigated through photoluminescence (PL) spectroscopy. In the case of the 4 M H_3PO_4 electrolyte, no perceptible growth of nanotubes was observed. The individual electrolytes of 0.3 M NH_4F and 1 M HF resulted into the formation of the wall-connected nanotubes. In contrast, the mixed electrolytes comprising the strong (NH_4F, HF) and weak (H_3PO_4) electrolytes have been found to be efficient for the growth of wall-separated titania nanotubes. The results of the PL spectroscopy have demonstrated that the free-standing nanotubes offer low PL intensity compared to its connected counterpart owing to the lower carrier recombination rate of free-standing nanotubes.

Key words: Titanium dioxide, anodization, mixed electrolytes, free-standing nanotube array, photoluminescence spectroscopy

INTRODUCTION

Nanoscale structures of titanium dioxide (TiO_2) have drawn significant scientific and technological attention due to their unique functional properties, useful for a wide range of domestic and industrial devices.[1] Among the popular techniques, electrochemical anodization has been found to be a potential one for the synthesis of different nanoscale structures (e.g., nanoporous, nanotubes, etc.).[2] Anodically grown TiO_2 nanotubes are widely used in sensors (e.g., biosensor[3] and gas sensor[4]) and photocatalytic (e.g., solar cell[5,6]) applications. The superior optoelectronic performance of the TiO_2 nanotube has been attributed to its one-dimensional channel-assisted carrier transportation, leading to a significantly reduced recombination of electron–hole.[4] The reduced tube wall thickness along with the increased length and separation between the tubes are conducive to the reduction in the recombination rate of photo-generated carriers.[7] Moreover, reduction of the barrier layer at the bottom of the free-standing nanotubes enhances the electron transport efficiency. The aforesaid merits allow the identification of free-standing ordered nanotube structures as the potential candidates for gas sensing application.

Earlier, TiO_2 thin films were prepared by using different types of electrolytes, viz., (1) fluoride based electrolytes like HF,[8] NH_4F,[6] NaF,[9] KF,[10] (2) sulphate based electrolytes like H_2SO_4,[11] $(NH_4)_2SO_4$,[1] Na_2SO_4,[12] (3) phosphate based electrolytes like

(Received August 20, 2013; accepted April 11, 2014; published online May 28, 2014)

H_3PO_4,[2] and (4) chlorine-based electrolyte, like $HClO_4$.[13] Various weak acids like oxalic acid[14] and acetic acid[15] have also been well investigated. The formation of self-ordered, highly oriented TiO_2 nanotube structures, by controlling the growth parameters like anodization time, applied potential, electrolyte compositions and concentrations, pH value of the electrolytes, bath temperature, and type of electrolytes, have also been reported.[8–16] Such efforts led to the controlled porosity of the film, nanotube length, inner radius of the pore/tube, wall thickness of the tube, tube separation, and stoichiometric profile. Recently, anodization by using mixed electrolyte has been found to be promising for the growth of controlled nanotube structures.[5] Among the various combinations, the fluorine-based electrolytes have been found to be the most efficient in forming the nanotube structures.[6] So far, different mixed electrolytes, like $(NH_4)_2SO_4$ with NH_4F, H_2SO_4 with HF,[1] H_3PO_4 with NaF[9] and H_3PO_4 with HF,[17] have been attempted. Lue et al.[5] have investigated ordered titania nanotube formation using NH_4F with H_3PO_4, in which the concentration of NH_4F was changed from 1 M to 7 M maintaining the H_3PO_4 concentration at 0.2 M. Usually, the fluoride-based strong electrolyte offers a high oxide dissolution rate compared to the growth rate, whereas a weak electrolyte offers a very slow oxide dissolution rate with high growth rate.[18] Earlier, the authors reported the formation mechanism of the free-standing TiO_2 nanotubes combining the effect of fluoride-based strong electrolyte and the soft electrolyte (H_3PO_4).[18]

The present study aims to investigate the detailed structural (XRD, FESEM) and optical [photoluminescence (PL)] properties of the connected nanotube arrays grown by using weak (H_3PO_4), strong (NH_4F and HF), and mixed (NH_4F with H_3PO_4 and HF with H_3PO_4) electrolytes. The results of structural characterisations have revealed that, in the case of mixed electrolytes (compared to the weak or strong electrolytes), the inner pore diameter, separation between the adjacent tubes, and the length of the tube increase with concomitant reduction in the tube wall thickness leading to a significant improvement of the aspect ratio (tube length:pore diameter) of the nanotubes. On the other hand, analysis of the PL spectra shows that the free-standing nanotubes offer lower PL intensity compared to its connected counterpart which is indicative of the low carrier recombination of free-standing nanotubes compared to the connected ones. Moreover, the connected nanotubes showed high energy oxygen vacancy (OV) peaks compared to the free-standing ones that may be attributed to the defect-induced trap-assisted recombination.[19]

EXPERIMENTAL

A highly ordered TiO_2 nanotube array was synthesized by an electrochemical anodization process. High purity titanium sheet (99.5%; Alfa Aesar, USA) having a dimension of 16 mm × 11.5 mm × 0.25 mm was used as the starting anode material/substrate during electrochemical anodization. The Ti substrate was cleaned thoroughly using acetone, ethanol, diluted hydrochloric acid, and deionised water (resistivity ~18.2 MΩ cm). Electrochemical anodization was carried out at room temperature using the 'two-electrode' configurations in a Teflon cell. A cylindrical-shaped graphite electrode (radius: 0.25 cm, surface area: 8.547 cm^2) was used as the counter electrode (cathode). The distance between the two electrodes was maintained at ~4 cm during the experiments. A constant potential of 20 V was applied using the Agilent U8002A single output DC power supply. A multimeter with computer interfacing facility was used for continuous recording of the current through the electrolyte during the anodization process. Each anodization process was carried out for a constant time of 120 min. The anodization process was carried out separately using the five different electrolytes, viz., aqueous solution of (1) 4 M H_3PO_4, (2) 1 M HF, (3) 0.3 M NH_4F, (4) 0.3 M NH_4F with 1 M H_3PO_4, and (5) 1 M HF with 1 M H_3PO_4. Analytical grade chemicals were used for all the experiments. Two of the anodization processes were performed using the mixed electrolytes of H_3PO_4 with NH_4F and H_3PO_4 with HF keeping all the other parameters unchanged. H_3PO_4 was considered as the weak electrolyte to grow continuous TiO_2 film as it provides excess amounts of phosphate ions (e.g., $H_2PO_4^-$, HPO_4^{2-}, PO_4^{3-}) which are easily adsorbed on the oxide surface during the electrochemical anodization process.[3,18] Figure 1a shows the schematic of the anodization setup.

The phase analysis of the grown TiO_2 nanotube was carried out at λ = 1.54 Å using x-ray diffractometry by maintaining the 2θ scan rate of 0.33°/min. Surface morphology of the TiO_2 nanotubes was characterized using a field emission scanning electron microscopy (FESEM). Optical characterizations of the different TiO_2 nanotube structures were carried out using PL spectroscopy, using a 450-W xenon lamp source. PL emission spectra were detected by a R928P photon-counting detector capable of detecting 250–900 nm wavelength.

RESULTS AND DISCUSSION

Variation of the current density as the function of anodization time is shown in Fig. 1b for five different electrolytes. During the initial stage of the anodization process, current density decreases rapidly for all the electrolytes, owing to the initial growth of a highly resistive oxide layer.[20] Subsequently, the nanotube formation process continues, through the combination of oxide growth and oxide dissolution (chemical and field-assisted dissolution[18]), in the case of fluoride-based electrolyte(s) [i.e., NH_4F, HF, NH_4F with H_3PO_4 and HF with H_3PO_4]. In this process, some fraction of the grown

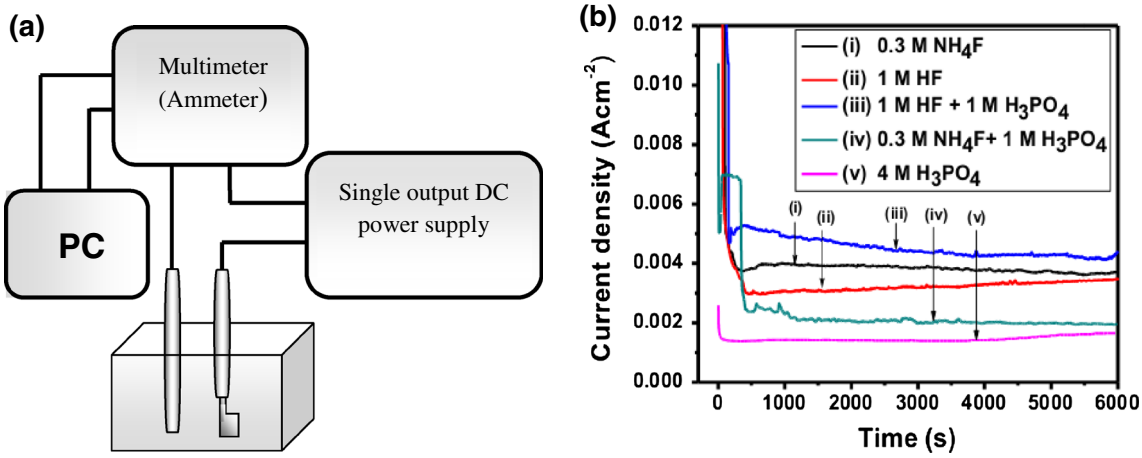

Fig. 1. (a) Schematic of the anodization setup. (b) Current density as a function of anodization time for different electrolytes.

oxide dissolves into the electrolyte, momentarily exposing the bare Ti surface. This is manifested by the corresponding increase in the current during the initial phase. Eventually, the dissolution and oxide formation processes reach an equilibrium and the current tends to saturate, as is evidenced by almost imperceptible undulations in the steady state value of the current. Tha absense of any abrupt increase in the current during the initial phase, as observed in the case of H_3PO_4, indicates that H_3PO_4 does not support the combined effect of oxidation and dissolution, which is the essential condition for nanotube formation.[18]

The x-ray diffraction (XRD) patterns of the anodically grown TiO_2 layer are shown in Fig. 2. It is evident that the anatase crystallinity with (101) peaks are common for all the five cases (according to the JCPDS File No. 21-1272). The anatase (204) peaks[21,22] are observed only for the TiO_2 nanotubes prepared by using HF or HF with H_3PO_4 electrolytes (Fig. 2c, e). All the high intensity Ti peaks, like (002), (101), (102), (103), and (112) (JCPDS 44-1294), are common for all the five different samples due to the use of same Ti substrate for the entire anodization process. Additionally, a very weak Ti (100) peak is observed only for the TiO_2 nanotube samples prepared by H_3PO_4, NH_4F and NH_4F with H_3PO_4 electrolytes (Fig. 2a, b, d).

Field emission scanning electron micrographs (FESEM) of the samples grown by using five different electrolyte(s) are shown in Fig. 3a–e. It is apparent from Fig. 3a that the 4 M H_3PO_4, electrolyte is not conducive for the growth of nanotube arrays. In the cases of the strong electrolyte, viz., aqueous solution of NH_4F (0.3 M) and HF (1 M), connected (without distinct wall separation) nanotubular array has been found to form as shown in Fig. 3b and c. In the case of mixed electrolytes [NH_4F (0.3 M) with H_3PO_4 (1 M)] and [HF (1 M) with H_3PO_4 (1 M)], formation of the free-standing, wall-separated highly oriented nanotube structure is clearly evident in Fig. 3d, e. The figures also

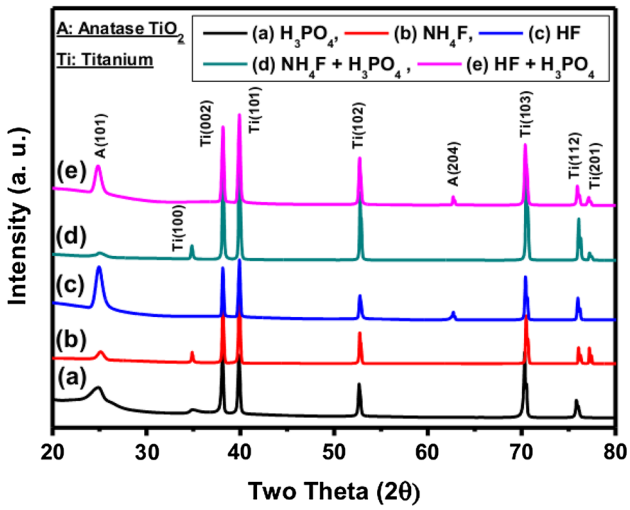

Fig. 2. XRD pattern of anodically grown TiO_2 nanotube array (using 20 V potential for 2 h) using different electrolytes: (a) 4 M H_3PO_4, (b) 0.3 M NH_4F, (c) 1 M HF, (d) 0.3 M NH_4F with 1 M H_3PO_4, (e) 1 M HF with 1 M H_3PO_4.

reveal the reduced wall thickness and higher separation between the adjacent tubes (with higher tube diameter) in the cases of mixed electrolytes compared to the single electrolytes. All the average structural dimensions, e.g., pore diameter, tube wall thickness, and separation between two tubes for different samples, were measured from the FESEM images (Fig. 3a–e) and are summarized in Table I. The length of the nanotubes was measured from cross-sectional FESEM images of the samples. Figure 3f shows a sample cross-sectional view for measuring the tube length in the case of an electrolyte consisting of 0.3 M NH_4F and 1 M H_3PO_4.

The presence of the OVs and sub-oxide states associated with different TiO_2 nanotube structures was investigated using the PL spectroscopy. The PL spectra of different nanotube structures were recorded after exciting the samples with 300 nm UV radiation, and the emission spectra were collected in

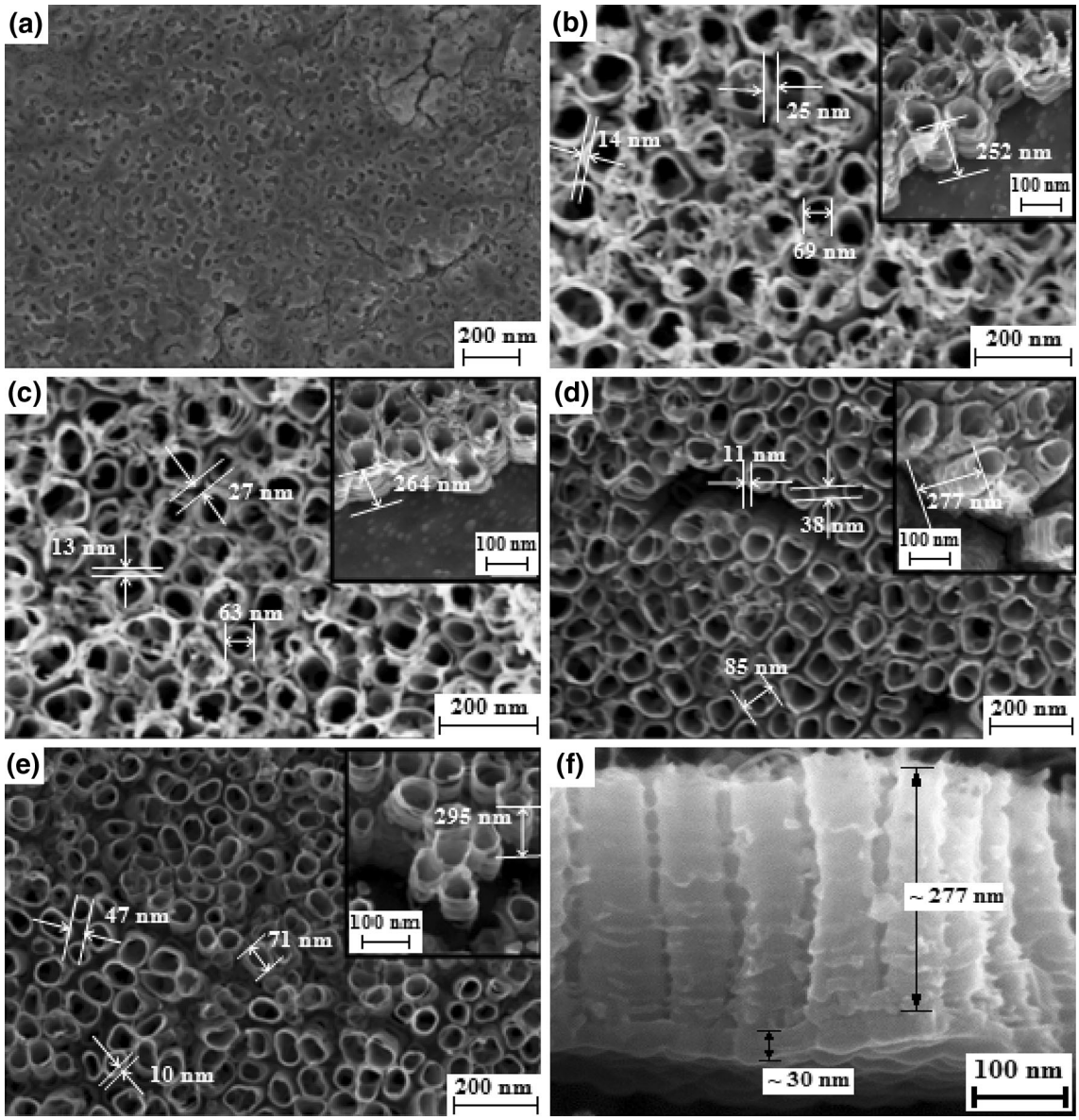

Fig. 3. FESEM images of an anodically grown TiO_2 nanotube array using 20 V potential for 2 h using different electrolytes (tilted view shown in inset). (a) 4 M H_3PO_4, (b) 0.3 M NH_4F, (c) 1 M HF, (d) 0.3 M NH_4F with 1 M H_3PO_4, (e) 1 M HF with 1 M H_3PO_4, (f) cross-sectional view of TiO_2 nanotube using 0.3 M NH_4F with 1 M H_3PO_4 electrolyte.

Table I. Average dimensions of nanotubular structure of anodically grown TiO_2 using different electrolytes

Electrolyte(s)	Inner diameter of pore (nm)	Tube wall thickness (nm)	Separation between two tubes (nm)	Tube length (nm)
4 (M) H_3PO_4	–	–	–	–
0.3 (M) NH_4F	69	14	25	252
1 (M) HF	63	13	27	264
0.3 (M) NH_4F with 1 (M) H_3PO_4	85	11	38	277
1 (M) HF with 1 (M) H_3PO_4	71	10	47	295

the wavelength range of 325–650 nm as shown in Fig. 4a, b. The excitation wavelength was chosen from the PL excitation spectrum (not shown here). The observations from the PL spectra of the samples (Fig. 4a) may be depicted as: (1) a very sharp PL peak is centred at ~470 nm; (2) the intensity of the

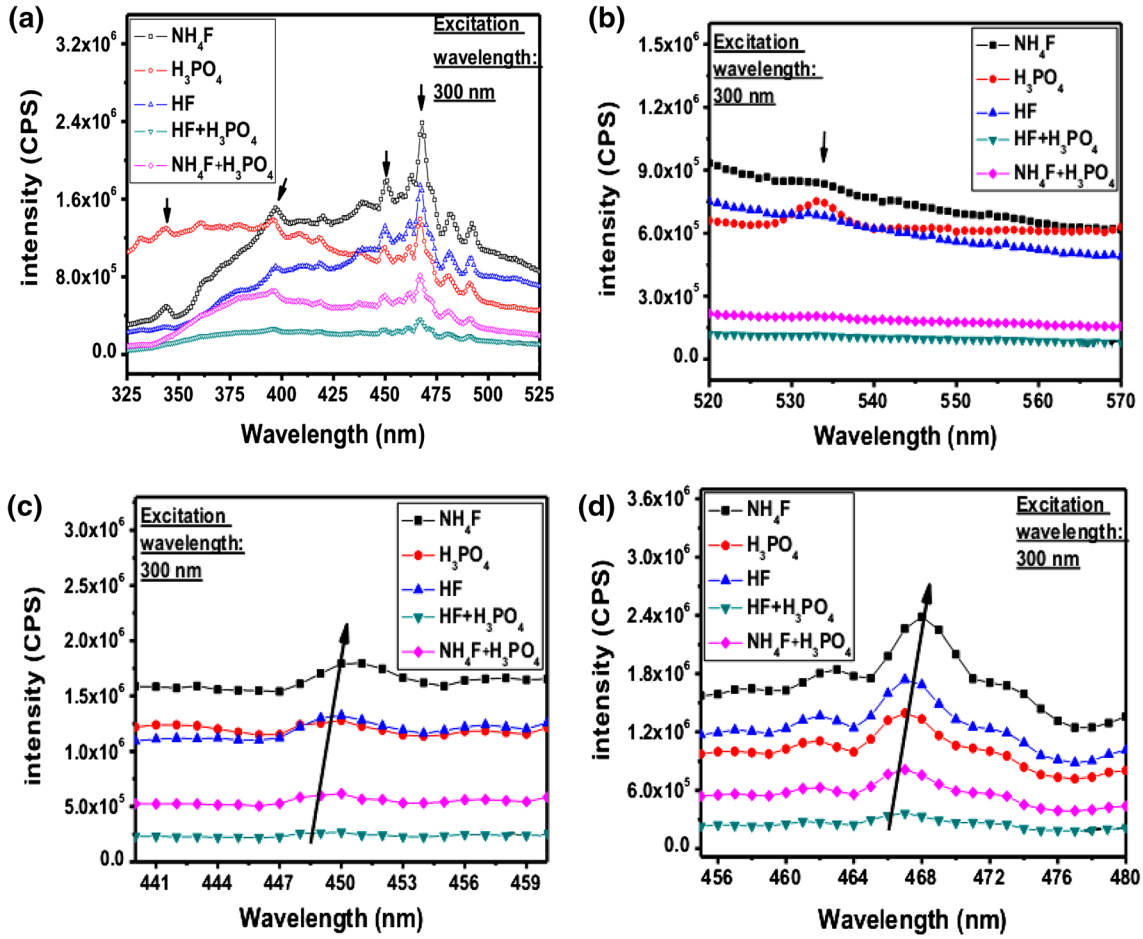

Fig. 4. PL spectra of (a) anodically grown five different TiO_2 structures using an excitation wavelength of 300 nm, (b) emission due to self-trap excitation, (c) blue shifts, (d) green shifts for NH_4F and HF electrolyte-based TiO_2 nanotubes.

peaks decreases with increase in separation of the nanotubes; (3) multiple peaks appear as the shoulders on the higher energy side (in the wavelength range of 425–500 nm) of the dominant peak at 470 nm; (4) the intensity of these peaks decreases with increase in separation of the nanotubes and become almost indistinguishable for the wall-separated free-standing nanotubes; (5) an additional high energy peak at 395 nm is common for both the connected and wall-separated nanotubes (these peaks are relatively weaker for the free-standing nanotubes) (6) a peak at 343 nm is identifiable only for the connected nanotube samples; (7) TiO_2 shows a broad high energy hump centred around 380 nm for the H_3PO_4 which is absent for other electrolytic samples, and (8) two spikes at lower energy side of the dominant peak appear at ~480 nm and 490 nm for all the samples and exhibit a trend similar to the higher energy shoulders, i.e. their intensity decreases with increase in separation of the nanotubes.

In general, it was observed that the interconnected nanotubes result in higher intensity PL peaks compared to the mixed electrolyte-based free-standing nanotubes. However, the decrease in PL intensity could be due to the decrease in density for the wall-separated nanotubes as the spot size of the excitation is constant. Additionally, the anodically grown porous TiO_2 film in the case of H_3PO_4 exhibits a different trend in comparison to the other samples, in which a broad hump in the PL spectrum in the higher energy region, with substantially high intensity, is observed. Such a trend is absent for all the other samples.

It is imperative to mention here that the PL emission is the result of the recombination of excited electron–hole pairs. When the external energy is applied to the semiconducting oxide, electrons are excited and transferred to the excited states. Emission spectra are found when the excited electrons are returned from their unstable excited state to lower energy states.[7] Mixed electrolyte-based free-standing TiO_2 nanotube structures show effectively a low intensity PL emission peak compared to the connected nanotubes grown by using fluoride-based strong electrolytes. This phenomenon indicates that the carrier recombination rate is effectively reduced for the free-standing nanotube structure compared to the other cases. Different energy states are introduced in the visible region due to the defect level formation by OVs in the TiO_2.

A high intensity PL peak at 470 nm (2.64 eV) is observed due to carrier trapping by OVs (Fig. 4a) as reported earlier by Wu et al.[7] Further, Janotti et al.[23] reported a detailed study on such OVs. High intensity PL emission peaks in the wavelength range of 440–500 nm indicate that the recombination process occurs via defect levels (different OVs state) rather than direct band to band recombination. So, the trap (single or multiple)-assisted recombination is also supported by the spike, like high intensity peaks in the visible region as evident from Fig. 4a. The presence of excess amounts of OVs in the anodically grown TiO_2 films has earlier been reported.[9,24] It has also been found that different sub-oxides (Ti_nO_{2n-1}), like Ti_2O_3, TiO etc., also form in anodically grown TiO_2 thin films.[25] These sub-oxide layers exist near the metal–oxide interface region and form a barrier layer. The concentration of oxygen decreases continuously towards the metal–TiO_2 interface and the highest OV concentrations are observed near to the barrier layer.[18,24] The peak at ~450 nm showed a significant blue shift owing to increase of energy level due to the contribution from OVs (Fig. 4c). On the other hand, a blue to green shift as observed in Fig. 4d, which is due to the higher concentrations of OVs that possibly increases the donor states near the conduction band.[26] In a separate study, Liu et al.[27] established the influence of defect states on the PL spectra in the cases of three types of TiO_2 nanotube, viz., as-grown, N_2 annealed at 400°C, and O_2 annealed at 400°C. The temperature-dependent PL spectrum revealed the appearance of a higher wavelength (>495 nm i.e. green region) emission peak for the N_2-annealed sample in contrast to the comparatively lower wavelength (<495 nm, i.e. blue region) PL emission peak for O_2 annealed TiO_2 nanotube. They concluded that OV concentrations must be higher for the N_2-annealed samples due to the thermal decomposition of TiO_2 in an oxygen-free environment compared to the O_2-annealed ones. Similar results have also been obtained in the present study indicating the appearance of the higher intensity PL emission peaks in the violet, blue, and green regions due to the wide distribution of OV states.

A high intensity UV emission spectrum corresponds to the band edge emission of bulk anatase TiO_2.[28,29] Both the emission peaks at 3.62 eV and 3.14 eV indicate the band to band recombination process of anatase TiO_2.[26] The UV-emission peak at 3.14 eV indicates the indirect band-gap energy for the bulk anatase phase,[30] whereas the 3.62 eV peak indicates the highest energy direct transition. Similar types of direct (3.66 eV) and indirect (3 eV) energy band gaps of TiO_2 nanotubes were reported by Shreekanta et al.[26] Photocatalytic activity of the anatase TiO_2 thin film is principally dominated by three important physical phenomena,[31] e.g., self-trapped excitation (STE),[32] OVs,[33,34] and surface imperfections.[27] Watanabe and Hayashi[32] and Iijima et al.,[19] in their attempts to measure the luminescence spectrum of anatase TiO_2 found a STE peak near 2.3 eV. In our present study, a small line-width emission at 534 nm (2.32 eV) can be attributed to the recombination of STE as shown in Fig. 4b. A high intensity STE peak is observed for the H_3PO_4-based anodic oxide sample and comparatively low intensity peaks are observed at the same wavelength for nanotube samples prepared by NH_4F and HF electrolytes. On the other hand, no self-trap excitation peaks are found for the mixed electrolyte-grown samples in the same band gap region as revealed in Fig. 4b.

Due to the presence of sufficient defect levels originated from OVs, all the nanotube structures showed high intensity PL peak(s) in the visible range. This indicates that the TiO_2 nanotubes are also suitable for solar cell applications because the solar spectrum contains only 5% of UV light.[7] The remarkably lower PL intensity of the free-standing TiO_2 nanotubes compared to that of the connected ones clearly indicates that the recombination of photo-generated electrons and holes was suppressed effectively in the case of free-standing nanotubes. It has been reported that the nanotubular structure (or any 1D geometrical structure) can trap more photon energy due to its one-dimensional structure where the carrier diffusion length is of the order of the nanotube length.[35] This facilitates the collection of the free carriers and therefore increases the total energy collection efficiency of the material. So, the one-dimensional carrier transport can be restricted due to the connected nature of the nanotubes where the photo-generated carriers are scattered or distributed to the connected neighboring nanotubes, reducing the effective carrier transport efficiency.

CONCLUSION

The present study demonstrates the growth of free-standing TiO_2 nanotubes by using a mixed solution comprising strong (NH_4F, HF) and weak electrolytes (H_3PO_4). The use of only the soft electrolyte (H_3PO_4) for anodization does not result in the growth of nanotube. The use of fluoride-based electrolytes (NH_4F and HF) gave rise the formation of connected TiO_2 nanotubular structures (with anatase ⟨101⟩ preferential growth) with indistinct wall separation. The use of mixed electrolytes (NH_4F with H_3PO_4 and HF with H_3PO_4) resulted in the formation of free-standing, wall-separated distinct TiO_2 nanotube arrays. By the combined effect of soft and strong (fluoride-based) electrolytes, oxide growth and dissolution became more controlled compared to that of the fluoride-based electrolyte. Low intensity PL emission peaks indicate that the free-standing nanotubes are suitable for solar cell and gas sensor applications due to the reduced carrier recombination rate compared to the their connected counterparts.

ACKNOWLEDGEMENTS

This work was supported in part by CSIR (Sanction letter No. 22(0518)/10/EMR-II), Department of

Science and Technology (Fast Track Scheme for Young Scientist: Sanction Letter No. SR/FTP/ETA-041/2011), AICTE Career Award for Young Teachers (Sanction letter No. 1-51/RIFD/CA/1/2011-12), Government of India and Indian National Science Academy (INSA) (Sanction letter No. SP/YSP/81/2013/735). A. Hazra gratefully acknowledges the Department of Science and Technology (DST), Govt. of India for providing INSPIRE Fellowship for pursuing his PhD degree. K. Dutta and B. Bhowmik gratefully acknowledge COE, TEQIP—II, Indian Institute of Engineering Science and Technology (IIEST), Shibpur, for their fellowship for pursuing PhD programme. Authors from BITS Pilani acknowledge UGC and DST, India, for their support. The authors sincerely acknowledge Dr. Mallar Ray, School of Materials Science and Engineering, Indian Institute of Engineering Science and Technology (IIEST), Shibpur, Howrah 711 103, India, for providing the facility of PL spectroscopy.

REFERENCES

1. J.M. Macak and P. Schmuki, *Electrochim. Acta* 52, 1258 (2006).
2. J. Choi, R.B. Wehrspohn, J. Lee, and U. Gösele, *Electrochim. Acta* 49, 2645 (2004).
3. E. Krasicka-Cydzik, *Biomater. Eng.* 7–8, 26 (1999).
4. G. Liu, K. Wang, N. Hoivik, and H. Jakobsen, *Sol. Energy Mater. Sol. Cells* 98, 24 (2012).
5. R. Liu, W.-D. Yang, L.-S. Qiang, and J.F. Wu, *Thin Solid Films* 519, 6459 (2011).
6. H. Yanga and C. Pan, *J. Alloy. Compd.* 492, L33 (2010).
7. F. Wu, X. Hu, J. Fan, E. Liu, T. Sun, L. Kang, W. Hou, C. Zhu, and H. Liu, *Plasmonics* 8, 501 (2013).
8. V.C. Anitha, D. Menon, S.V. Nair, and R. Prasanth, *Electrochim. Acta* 55, 3703 (2010).
9. K.S. Raja, M. Misra, and K. Paramguru, *Electrochim. Acta* 51, 154 (2005).
10. R.P. Antony, T. Mathews, A. Dasgupta, S. Dash, A.K. Tyagi, and B. Raj, *J. Solid State Chem.* 184, 624 (2011).
11. S.K. Hazra and S. Basu, *Sens. Actuators B* 115, 403 (2006).
12. J.M. Macak, K. Sirotna, and P. Schmuki, *Electrochim. Acta* 50, 3679 (2005).
13. R.P. Antony, T. Mathews, C. Ramesh, N. Murugesan, A. Dasgupta, S. Dhara, S. Dash, and A.K. Tyagi, *Int. J. Hydrogen Energy* 37, 8268 (2012).
14. F.T. Cheng, P. Shi, G.K.H. Pang, M.H. Wong, and H.C. Man, *J. Alloy. Compd.* 438, 238 (2007).
15. O. Sanz, F.J. Echave, J.A. Odriozola, and M. Montes, *Ind. Eng. Chem. Res.* 50, 2117 (2011).
16. M.K. Jackson and W. Ahmed, *Surface Engineered Surgical tools and Medical Device* (New York: Springer Science, 2007), pp. 21–47.
17. H. Tsuchiya, J.M. Macak, L. Taveira, E. Balaur, A. Ghicov, K. Sirotna, and P. Schmuki, *Electrochem. Commun.* 7, 576 (2005).
18. A. Hazra, B. Bhowmik, K. Dutta, V. Manjuladevi, R.K. Gupta, P.P. Chattopadhyay, and P. Bhattacharyya, *Sci. Adv. Mater.* 6, 714 (2014).
19. K. Iijima, M. Goto, S. Enomoto, H. Kunugita, K. Ema, M. Tsukamoto, N. Ichikawa, and H. Sakama, *J. Lumin.* 128, 911 (2008).
20. S. Minagar, C.C. Berndt, J. Wang, E. Ivanova, and C. Wen, *Acta Biomater.* 8, 2875 (2012).
21. R.A. Antunes, M.C.L. de Oliveira, and M.F. Pillis, *Int. J. Electrochem. Sci.* 8, 1487 (2013).
22. J.M. Macak, H. Tsuchiya, A. Ghicov, K. Yasuda, R. Hahn, S. Bauer, and P. Schmuki, *Curr. Opin. Solid State Mater. Sci.* 11, 3 (2007).
23. A. Janotti, J.B. Varley, P. Rinke, N. Umezawa, G. Kresse, and C.G. Van de Walle, *Phys. Rev. B* 81, 085212 (2010).
24. A.G. Mantzila and M.I. Prodromidis, *Electrochim. Acta* 51, 3537 (2006).
25. J. Marsh and D. Gorse, *Electrochim. Acta* 43, 659 (1998).
26. S. Sreekantan, K.A. Saharudin, Z. Lockman, and T.W. Tzu, *Nanotechnology* 21, 365603 (2010).
27. L.Z. Liu, W. Xu, X.L. Wu, Y.Y. Zhang, T.H. Chen, and P.K. Chu, *Appl. Phys. Lett.* 100, 121904 (2012).
28. B. Choudhury and A. Choudhury, *J. Lumin.* 132, 178 (2012).
29. A. Peng, E. Xie, C. Jia, R. Jiang, and H. Lin, *Mater. Lett.* 59, 3866 (2005).
30. P.J. Dihingia and S. Rai, *J. Lumin.* 132, 1243 (2012).
31. M. Yang, W. Liu, J.-L. Sun, and J.-L. Zhu, *Appl. Phys. Lett.* 100, 043106 (2012).
32. M. Watanabe and T. Hayashi, *J. Lumin.* 112, 88 (2005).
33. Y. Yang, X. Wang, C. Sun, and L. Li, *J. Appl. Phys.* 105, 094304 (2009).
34. I. Sildos, A. Suisalu, J. Aarik, T. Sekiya, and S. Kurita, *J. Lumin.* 87, 290 (2000).
35. N. Han, F. Wang, and J.C. Ho, *Nanomater. Energy* (2011). doi:10.1680/nme.11.00005.